Desalination and Water Treatment
www.deswater.com

doi:10.5004/dwt.2017.0441

69 (2017) 217–228
March

Comparative performance evaluation of LT-MEE desalination systems with three feed configurations

Shihe Zhou, Shengqiang Shen*, Yali Guo, Xingsen Mu

Key Laboratory of Liaoning Province for Desalination, School of Energy and Power Engineering, Dalian University of Technology, China, emails: zhoushihe2006@163.com (S. Zhou), zzbshen@dlut.edu.cn (S. Shen), ylguo@dlut.edu.cn (Y. Guo), magicruby@gmail.com (X. Mu)

Received 20 April 2016; Accepted 19 June 2016

ABSTRACT

Horizontal-tube falling-film evaporator has been widely applied in the low-temperature multi-effect evaporation (LT-MEE) desalination system because of its unique advantages. Research shows that the spray density has a significant effect on the heat transfer effect of this kind of evaporator and it is closely related to the feed configuration. Therefore, this paper focused on the feed configurations suitable for the large-scale LT-MEE desalination plant based on a reasonable spray density, which include the parallel feed and mixed feed. Based on the mass and energy conservation equations, the corresponding mathematical models were established, which consider the thermodynamic losses including boiling point elevation (BPE), non-equilibrium allowance inside evaporators/condensers and distillate flashing boxes, and flow resistances from evaporation to condensation. Validity of the model was verified through comparison between the industrial data. The effects of heating steam temperature and number of effects on the performance parameters were investigated. The comparison of performance and scaling tendencies between various feed configurations was accomplished. Results show that the mixed feed system presents a better performance than the parallel feed systems, while scaling risk of the combination of backward and parallel feed configuration is the highest. This comparison illustrates the logic behind choosing each feed configuration.

Keywords: Desalination; Multi-effect evaporation; Parallel feed; Mixed feed

1. Introduction

Desalination industry has expanded rapidly during the past few decades. The total desalination capacity is about 85.96 million m^3/d worldwide and about 1 million m^3/d in China [1]. The commercial desalination technologies can be divided into two main categories: thermal evaporation including multi-stage flash (MSF) and multi-effect evaporation (MEE), and membrane separation including reverse osmosis (RO). In the past, MEE suffered the scaling problem and high expenditure cost. However, new designs allow the system operating at lower top brine temperature (TBT) and using cheaper material solved this problem [2]. Therefore, the market share of MEE is growing rapidly, and the amount of its installed capacity has exceeded 8% of the total installed capacity around the world [3]. Meanwhile, MEE accounts for 39.6% of the total installed capacity in China [1].

According to different schemes for supplying the feed seawater to the evaporators, the possible configurations of MEE include the forward feed (FF), backward feed (BF), parallel feed (PF) and mixed feed. Most of the previous publications concentrated on performance analysis of the FF, BF and PF configurations. El-Dessouky et al. [4] conducted a comparative analysis of the FF and PF for MEE. Results show that the FF is more efficient than the other systems since it has the lowest specific power consumption, specific

*Corresponding author.

Presented at the EDS conference on Desalination for the Environment: Clean Water and Energy, Rome, Italy, 22–26 May 2016.

heat transfer area (SHTA) and specific cooling water flow rate. Darwish and Abdulrahim [5] compared the performances of FF, BF and PF. The conclusions are obtained that the BF configuration produces higher gained output ratio (GOR) and allows smaller specific hear transfer area. The rejected heat of all the three configurations decreases with the increase of number of effects and that of the BF is the least. Sharaf et al. [6] also carried out a comparative study of FF, BF and PF configurations. Results indicate that GOR of the FF is the lowest, and the PF is the optimal configuration when the number of effects is in the range of 16~18. In addition, the scale risk of BF is the highest because the maximum salinity occurs in the first effect, which has the highest evaporation temperature. Al-Mutaz and Wazeer [7] studied the three configurations above as well. Results show that the PF configuration, which has higher GOR and lower specific heat consumption, has better performance characteristics than the other two feed configurations.

It is worth noting that the horizontal-tube falling-film evaporator (HTE) has been extensively utilized in LT-MEE desalination system because of significant advantages, such as high heat flux under low liquid flow rate and small temperature difference [8,9]. For this type of evaporators, the spray density has an important influence on the heat transfer efficiency [10], and it is defined as the mass flow rate of seawater through one side of the horizontal tube per unit time and unit tube length as shown in Eq. (1):

$$\Gamma = \frac{M_f}{N \times L_t \times 2} \tag{1}$$

where M_f, N and L_t represent the mass flow rate of feed seawater, the number of tube column and the length of heat transfer tube, respectively.

Obviously, the mass flow rate of feed seawater is closely related to the spray density and influenced by the feed configuration. Therefore, on the premise that both the concentration ratio (CR) and the arrangement of tube bundle remain the same, the spray density is affected by the feed configuration of LT-MEE desalination system. Generally speaking, the FF or BF arrangement is only suitable for a small-scale LT-MEE desalination plant because it makes the mass flow rate of feed seawater into each effect of evaporator/condenser too large to ensure the spray density within a proper range for a large-scale plant. In the PF arrangement, the feed seawater is equally divided into each effect so that the amount of feed seawater sprayed for each effect is relatively small, especially in the case of large number of effects. As a result, the total amount of feed seawater can only vary in a relatively small range in order to prevent a dry area occurring on the surface of heat transfer tube and affect the stable operation of desalination plant. The mixed feed configuration includes two modes: the combination of FF and PF (FF&PF) or that of BF and PF (BF&PF). The mixed feed configuration is especially suitable for a large-scale LT-MEE desalination plant because of its flexibility.

Review of the literatures shows that the feed configuration has a significant influence on the design and performance of MEE desalination system. However, a limited number of publications involved the MEE desalination system with mixed feed configuration, and little consideration has been taken of the spray density to ensure a stable and good operation in the system analysis. In this paper, the suitable range of spray density was obtained by analyzing its effect on the performance of LT-MEE. On the base of the limitation of spray density, comparative performance evaluation of LT-MEE desalination system with three feed configurations were carried out, which included parallel, the combination of forward and parallel, and the combination of backward and parallel configuration. The effects of the number of effects and the temperature of heating steam on the performance parameters were studied. In addition, the scaling tendencies of various feed configurations were analyzed as well.

2. Process description

The process schematics of LT-MEE with the PF and mixed feed configurations are shown in Figs. 1–3, respectively.

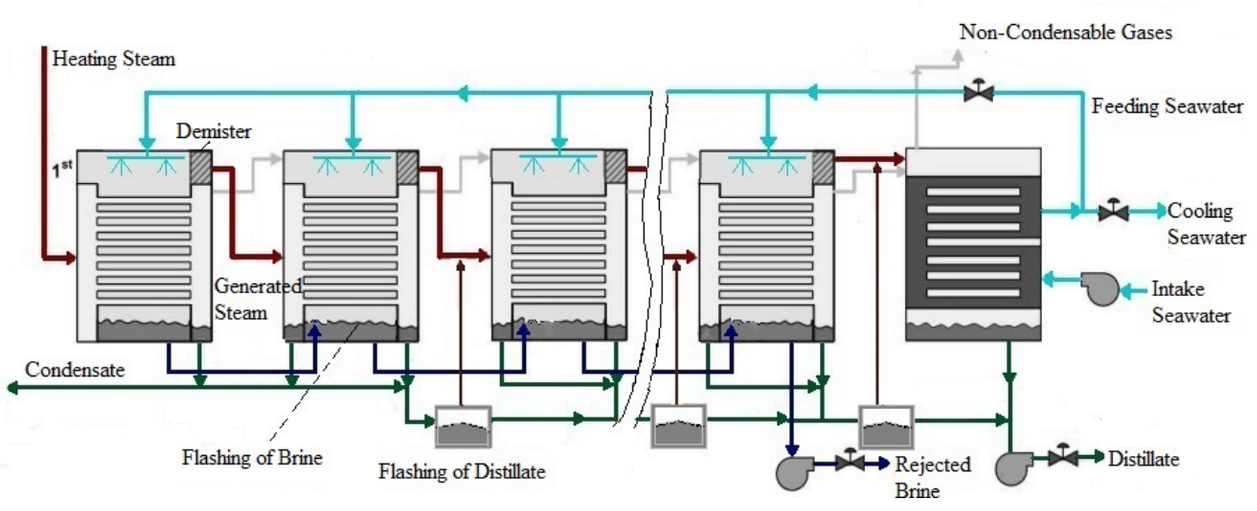

Fig. 1. Schematic of LT-MEE with the PF configuration.

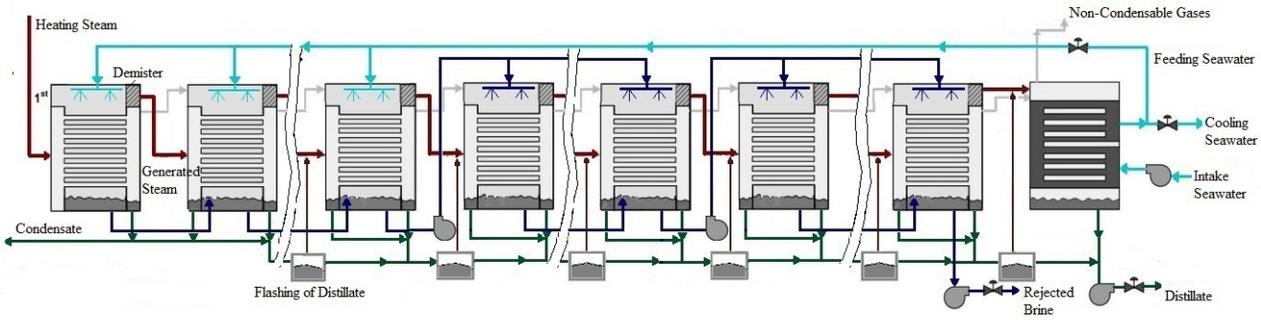

Fig. 2. Schematic of LT-MEE with the mixed feed configuration of FF&PF.

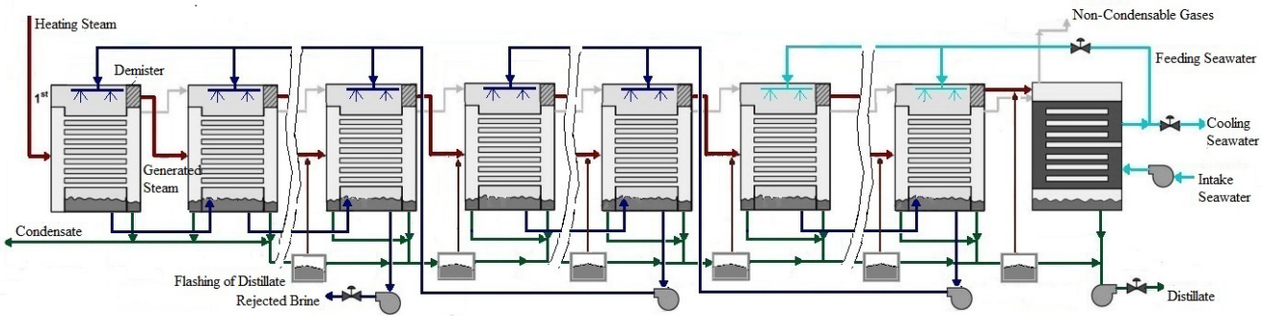

Fig. 3. Schematic of LT-MEE with the mixed feed configuration of BF&PF.

Each system mainly contains an end condenser and a series of HTE. It is customarily known as effects numbered 1 to *n* from left to right in the figures. Each effect is consisted of tube bundle, vapor space, demister and other accessories. Other auxiliary equipment include distillate flashing boxes, a venting system, brine and distillate expelling, and seawater feeding facilities.

In the first effect, the heating steam from external heat source condenses inside the tube and supplies heat for the seawater preheating and evaporating. The condensate in the first effect of evaporator/condenser either returns to the boiler or flows into the distillate flashing box, which depends on the requirement of heat source. At the same time, a portion of the feed seawater is converted into vapor when it is heated to saturated state by the heating steam inside tubes. After that, the generated vapor flows into the tubes side of next effect as the heating steam through the demister. The vapor generated in the last evaporator/condenser condenses in the end condenser. The condensates from the last distillate flashing box and the end condenser are the product of desalination plant.

The intake seawater is introduced into the end condenser to cool the steam generated in the last evaporator/condenser. A part of the intake seawater is conducted to the system as the feed seawater, and the other part as the cooling water is discharged into the sea. As for the PF configuration shown in Fig. 1, flow direction of the feed seawater is perpendicular to that of the vapor. The feed seawater is equally allocated to each effect of evaporator/condenser, and then evenly sprayed onto the top row of heat transfer tubes by liquid distributor. The seawater falls in the form of thin film along the tube bundle while evaporating continuously. The remaining brine falls to the bottom of the tank and, afterwards, flows into the brine space of next effect with flashing because of the non-equilibrium allowance. This process repeats in the subsequent effects, and the brine is finally discharged at the last evaporator/condenser. In the mixed feed configurations, all the effects of evaporators/condensers are divided into several groups, and the PF is adopted within the same group. Depending on the feed arrangement between the groups, the mixed feed configurations are divided into two modes: the combination of FF and PF (Fig. 2) and the combination of BF and PF (Fig. 3).

3. Mathematical modeling

Mathematical models of the LT-MEE desalination system with various feed configurations above have been developed according to the conservations of energy, mass and salinity. An assumption is made that the system is in a stable operating state. Features of the developed mathematical models are as follows:

- Detailed considerations in the thermodynamic losses include boiling point elevation (BPE), non-equilibrium allowance inside the evaporators/condensers and the distillate flashing boxes, temperature depressions corresponding to flow resistances across the tube bundle, in the demister, vapor transmission channels and the condensation process.
- The physical properties of seawater are regarded as a function of temperature and salinity. And those of water and saturated steam as a function of temperature.

- Constant heat transfer area in all effects of evaporators/condensers is adopted in accordance with industrial design.

The mathematical model of PF configuration was presented in the previous work [11], and the differences between the mathematical models of the (FF&PF)/(BF&PF) and parallel configurations are shown as follows. The number of effects of LT-MEE system is denoted by n. All the evaporators/condensers are divided into m groups, and the number of effects in each group are n_1, ..., n_m, respectively.

The mass balance of evaporator/condenser is as follows:

$$M_{f,i} = M_{d,i} + M_{b,i} \quad i = 1, n_1 + 1, ..., \sum_{k=1}^{m-1} n_k + 1 \tag{2}$$

$$M_{f,i} + M_{b',i-1} = M_{b',i} + M_{d,i} + M_{bf,i} \quad i \in \{2, ..., n\}, i \neq n_1 + 1, ..., \sum_{k=1}^{m-1} n_k + 1 \tag{3}$$

In the (FF&PF) configuration,

$$M_{f,i} = M_f / n_1 \quad i \in \{1, ..., n_1\} \tag{4}$$

$$M_{f,i} = \left[M_f - \sum_{j=1}^{(n_1 + ... + n_{k-1})} \left(M_{d,j} + M_{bf,j} \right) \right] \Big/ n_k \quad i \in \{n_1 + 1, ..., n\}, k \in \{2, ..., m\} \tag{5}$$

In the (BF&PF) configuration,

$$M_{f,i} = M_f / n_m \quad i \in \{n - n_m + 1, ..., n\} \tag{6}$$

$$M_{f,i} = \left[M_f - \sum_{j=n-(n_{k+1} + ... + n_m)}^{n} \left(M_{d,j} + M_{bf,j} \right) \right] \Big/ n_k \quad i \in \{1, ..., n - n_m\}, k \in \{1, ..., m-1\} \tag{7}$$

The salinity balance of evaporator/condenser is as follows:

$$M_{f,i} X_{f,i} = M_{b,i} X_{b,i} \quad i = 1, n_1 + 1, ..., \sum_{k=1}^{m-1} n_k + 1 \tag{8}$$

$$M_{f,i} X_{f,i} + X_{b,i-1} M_{b',i-1} = X_{b,i} M_{b',i} \quad i \in \{2, ..., n\}, i \neq n_1 + 1, ..., \sum_{k=1}^{m-1} n_k + 1 \tag{9}$$

The energy balance of evaporator/condenser is as follows:

$$M_{hs} \lambda_{hs} = M_{f,1} \left(c_{pb,1} T_{b,1} - c_{pf,1} T_{f,1} \right) + M_{d,1} h_{d,1} \tag{10}$$

$$M_{d,i-1} \lambda_{d,i-1} + M_{df,i-1} \lambda_{df,i-1} + M_{bf,i-1} \lambda_{bf,i-1} = M_{f,i} \left(c_{pb,i} T_{b,i} - c_{pf,i} T_{f,i} \right) + M_{d,i} h_{d,i} \quad i \in \{2, ..., n\} \tag{11}$$

where M, X, c_p, λ, T and h represent the mass flow rate, salinity, specific heat at constant pressure, latent heat of condensation, temperature and specific enthalpy, respectively. The subscripts of *hs*, *f*, *b*, *d*, *b′*, *df* and *bf* stand for heating steam, feed seawater, brine, distillate, accumulated brine, distillate and brine flashing, respectively. It is worth noting that no flashing of brine occurs in the first effect of evaporator/condenser of each group because there is no accumulated brine flowing into it. The amount of steam produced by flashing of brine can be calculated according to the following equations:

$$M_{bf,i} = 0 \quad i = 1, n_1 + 1, ..., \sum_{k=1}^{m-1} n_k + 1 \tag{12}$$

$$M_{bf,i} \lambda_{bf,i} = \left(c_{pb,i} T_{b,i} - c_{pb,i-1} T_{b,i-1} \right) M_{b',i-1} = \left(c_{pb,i} T_{b,i} - c_{pb,i-1} T_{b,i-1} \right) \sum_{j=\sum_{k=1}^{x-1} n_k + 1}^{i-1} \left(M_{b,j} - M_{bf,j} \right) \quad i \in \{2, ..., n\}, i \neq n_1 + 1, ..., \sum_{k=1}^{m-1} n_k + 1, x \in \{1, ..., m\} \tag{13}$$

The calculations of some parameters deserve special attention in the LT-MEE desalination system with the HTE. The condensation temperature of the steam generated in the ith effect of evaporator/condenser is calculated by Eq. (14):

$$T_{c,i} = T_{b,i} - BPE_i - \delta T_{bun,i} - \delta T_{dem,i} - \delta T_{fri,i} - \delta T_{loc,i} - \delta T_{con,i} \tag{14}$$

where $T_{b,i}$ is the saturated temperature of brine in the ith effect. $\delta T_{bun,i}$, $\delta T_{dem,i}$, $\delta T_{fri,i}$, $\delta T_{loc,i}$ and $\delta T_{con,i}$ are the temperature depressions corresponding to flow resistances across the tube bundle, in the demister, vapor transmission channels and the condensation process, and BPE is the boiling point elevation of brine, detailed calculations of which can be seen in reference [12].

Since the feed seawater is supplied in the subcooled state, the heat transfer process in the evaporator/condenser is divided into two stages of preheating and evaporating. The heat transfer coefficients of preheating phase [13] are calculated by using Eq. (15):

$$U_{pre} = 1719.4 + 3.2 T_c + 1.6 \times 10^{-2} T_c^2 - 2 \times 10^{-4} T_c^3 \tag{15}$$

The basic form for the calculation equation of heat transfer coefficients of evaporating phase is as Eq. (16):

$$U_e = \frac{1}{\frac{1}{K_{out}} + \frac{d_{out}}{d_{in} K_{in}} + \frac{1}{2\pi\xi \ln\left(\frac{d_{out}}{d_{in}} \right)} + R_{fou}} \tag{16}$$

where d_{out} and d_{in} stand for the outer and inner diameters of heat transfer tube. ξ and R_{fou} are the resistances of thermal conductivity and fouling of tube wall, respectively. K_{out} is the heat transfer coefficient of falling-film evaporation outside the tube, and K_{in} is that of steam condensation inside the tube.

Two experiments were carried out to study the heat transfer coefficients of falling-film evaporation outside the

tube and condensation inside the tube, respectively, which were introduced in the work of Shen et al. [14,15]. Empirical correlations were obtained based on the data from those experimental studies with each correlation coinciding with the heat transfer and flow performances of individual experimental results, as follows:

$$K_{\text{out}} = \frac{0.0388 Re^{0.104} Pr^{1.1882} g^{1/3} k_{\text{sw}}}{\eta_{\text{sw}}^{2/3}} \tag{17}$$

where Re is Reynolds number, $Re = 4\Gamma/\mu$. Pr is Prandtl number, $Pr = 1000\mu c_{\text{p}}/k_{\text{sw}}$. k_{sw} and η_{sw} are the coefficients of thermal conductivity and kinematic viscosity of seawater, respectively:

$$K_{\text{in}} = 0.3\frac{2\pi-\theta}{2\pi}\left[\frac{\rho_{\text{v}}(\rho_{\text{l}}-\rho_{\text{v}})g\lambda k_{\text{l}}^3}{\mu_{\text{l}} d_{\text{in}}(T_{\text{c}}-T_{\text{wall}})}\right]^{\frac{1}{4}} \tag{18}$$

where k_l, ρ_l and μ_l are the coefficients of thermal conductivity, density and dynamic viscosity of condensate, respectively. ρ_v is the density of steam. g is the acceleration of gravity. T_{wall} is the temperature of tube wall. θ is the angle of liquid level.

Some evaluation parameters for LT-MEE desalination system are defined as follows. The CR is as follows:

$$\text{CR} = \frac{M_t}{M_{\text{f}} - M_{\text{d}}} = \frac{X_{\text{b}}}{X_{\text{f}}} \tag{19}$$

where M_d is the total distillate production of LT-MEE desalination system. X_f and X_b are the salinity of feed seawater and that of brine, respectively.

The GOR is as follows:

$$\text{GOR} = M_{\text{d}}/M_{\text{hs}} \tag{20}$$

where M_{hs} is the mass flow rate of the heat steam from an external heat source. GOR reflects the operating cost of the thermal desalination plant.

The SHTA as the evaluating criteria of the equipment cost is defined as follows:

$$\text{SHTA} = \left(A_{\text{con}} + \sum_{i=1}^{n} A_i\right) \Big/ M_{\text{d}} \tag{21}$$

where A_{con} and A_i are the heat transfer area of condenser and that of the ith effect of evaporator/condenser, respectively.

The definition of the specific cooling seawater (SCS) is as follows:

$$\text{SCS} = M_{\text{rej}}/M_{\text{d}} \tag{22}$$

where M_{rej} is the cooling seawater rejected back to the sea. SCS indicates the direct heat loss of condenser and determines the relative power of seawater pump.

4. Results and discussion

A computer program is developed based on the mathematical model of LT-MEE using Visual Basic 6.0, the algorithm flowchart of which was presented in the previous publication [11].

The validation of the simulation results was accomplished by comparing with the commercial plants as shown in Table 1. At the same given parameters, the relative errors of GOR are 2.24% and 1.08%, and that of SHTA is –2.95%. The simulation results of the model show a good agreement with the actual data. Thus, it can be verified that the calculation method is accurate and reliable for engineering design.

LT-MEE desalination system with the production capacity of 15,000 m^3/d is taken as the example to study the influences of number of effects and heating steam temperature on performance parameters of the desalination system with various feed configurations. The required input parameters are summarized in Table 2.

Average spray density $\Gamma_{a,i}$ of the ith effect of evaporator/condenser is defined as the arithmetic mean value of spray density $\Gamma_{\text{top},i}$ of top row and that $\Gamma_{\text{bottom},i}$ of bottom row of the ith effect of evaporator/condenser, as follows:

$$\Gamma_{\text{a},i} = \frac{\Gamma_{\text{top},i} + \Gamma_{\text{bottom},i}}{2} \tag{23}$$

Table 1
Mathematical model simulation against the commercial plant

Parameters	12-effect MEE		4-effect MEE-TVC[a]	
	Sidem [5]	Model	Huanghua [16]	Model
Capacity ($m^3 \cdot d^{-1}$)	12,009.6	12,009.6	10,000	10,000
Feed configuration	HTE-FF	HTE-FF	HTE-PF	HTE-PF
Salinity of feed seawater (ppm)	36,000	36,000	36,000	36,000
Salinity of rejected brine (ppm)	72,000	72,000	51,600	51,600
Heating steam temperature T_{hs} (°C)	69.8	69.8	65	65
Temperature in the last effect T_n (°C)	34.5	34.5	51.8	51.8
GOR	9.8	10.02	8.33	8.42
SHTA ($m^2 \cdot s \cdot kg^{-1}$)	N/A	508.72	352.1	341.7

[a]TVC: thermal vapor compressor.

Table 2
The required input parameters for the program

Parameters	Value	Parameters	Value
Production capacity ($m^3 \cdot d^{-1}$)	15,000	Heating steam temperature T_{hs} (°C)	56–72
Number of effect	6–12	Temperature in the last effect T_n (°C)	40
Seawater temperature (°C)	25	Row-column ratio of tube bundle	2.2
Seawater salinity X_f, (ppm)	32,000	Length of heat transfer tube L_t (m)	7.0
Temperature of feed seawater (°C)	35	Outer diameter of heat transfer tube (m)	0.025

Moreover, average spray density Γ_a of the LT-MEE desalination plant is expressed by the arithmetic mean value of average spray density $\Gamma_{a,i}$ of each effect of evaporator/condenser as shown below:

$$\Gamma_a = \frac{\sum_{i=1}^{n} \Gamma_i}{n} \tag{24}$$

Similarly, average heat transfer coefficient $K_{out,a}$ of evaporation outside the tube, average heat transfer coefficient $K_{in,a}$ of condensation inside the tube and average overall heat transfer coefficient $U_{e,a}$ of the LT-MEE desalination plant are defined as follows:

$$\Gamma_{in,a} = \frac{\sum_{i=1}^{n} \Gamma_{in,i}}{n} \tag{25}$$

$$K_{out,a} = \frac{\sum_{i=1}^{n} K_{out,i}}{n} \tag{26}$$

$$U_{e,a} = \frac{\sum_{i=1}^{n} U_{e,i}}{n} \tag{27}$$

Variations of $U_{e,a}$, $K_{out,a}$ and $K_{in,a}$ with Γ_a are shown in Fig. 4. It can be seen that with the increase of Γ_a, $K_{out,a}$ increases by deceleration and $K_{in,a}$ decreases slightly. Therefore, $U_{e,a}$ shows a tendency of increase, and the increasing rate decreases gradually. The enhancement of the falling film fluctuation improves the heat transfer for the flow velocity of feed seawater that increases with Γ_a at low spray density. Although the liquid film also thickens with Γ_a, the fluctuation still plays a dominating role. However, when the Γ_a continues increasing, the further increase in film thickness leads to a suppressing impact on the disturbance, and the increasing rate of $K_{out,a}$ diminishes.

Effects of the spray density on the performance parameters are shown in Fig. 5. With the increase of Γ_a, both GOR and SHTA show decline trends, and the decreasing rate of SHTA gradually reduces because of the variation of $K_{e,a}$. When Γ_a increases from 0.019 to 0.045 kg/(m×s), and then to 0.071 kg/(m×s), SHTA decreases by 11.5% and 3.4%, and GOR reduces by 10.8% and 11.1%, accordingly. It can be seen that the increase of Γ_a at low spray density will be helpful to improve the overall performance of the desalination plant. However, when the spray density Γ_a exceeds 0.07 kg/(m×s), its beneficial effect on the performance is very limited and even adverse.

Based on the analysis above, the minimum spray density of bottom row is set at 0.03 kg/(m×s), and the maximum spray density of top row is not more than 0.07 kg/(m×s) in the study later in this paper to ensure the average spray density of desalination plant in the proper range. As for the mixed feed configuration, the changing position of mixed point leads to different plans for a certain number of effects. Taking n = 11 of FF&PF for example, performance parameters of all the plans, which meet the limitations of spay density, vary with the positions of mixed points as shown

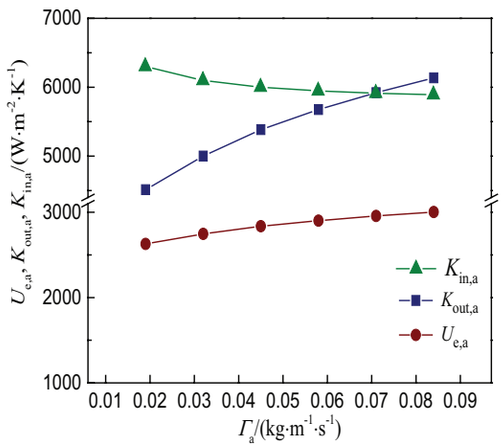

Fig. 4. Variations of $K_{e,a}$, $h_{out,a}$ and $h_{in,a}$ with Γ_a.

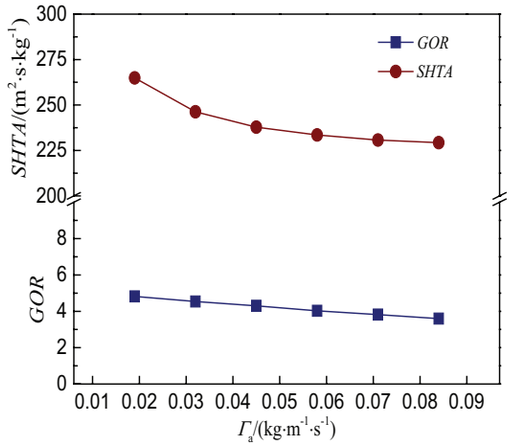

Fig. 5. Variations of SHTA and GOR with Γ_a.

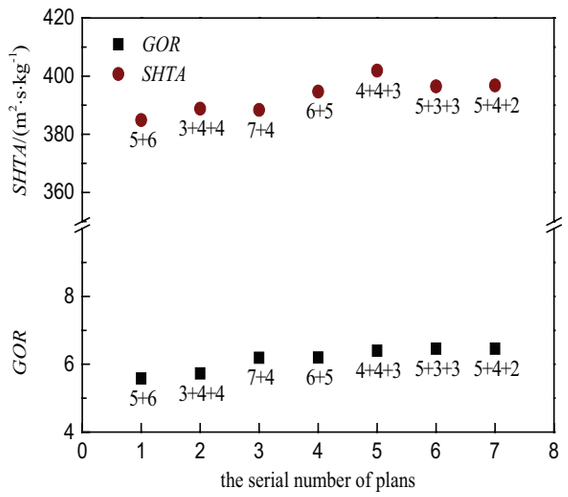

Fig. 6. Variations of the performance parameters with the position of mixed point for T_{hs} = 70°C and n = 11.

in Fig. 6. In this paper, GOR is regarded as the most important measure and followed by SHTA. From Fig. 6, it can be observed that the plan No. 6 obtains a better performance, which is denoted by (5 + 3 + 3) when the positions of mixed points are at the 5th and 8th effect, respectively. Therefore, in the same way with number of effects in the range of 6~12, the corresponding selected plans for the combination of FF and PF (FF&PF) are (4 + 2), (5 + 2), (4 + 2 + 2), (4 + 3 + 2), (5 + 3 + 2), (5 + 3 + 3) and (4 + 3 + 3 + 2), and that for the combination of BF and PF (BF&PF) are (3 + 3), (4 + 3), (2 + 3 + 3), (3 + 3 + 3), (3 + 3 + 4), (3 + 4 + 4) and (3 + 3 + 3 + 3).

Effects of number of effects on the performances of LT-MEE desalination system with three feed configurations are shown in Fig. 7. Fig. 7(a) shows the variations of CR of three feed configurations with the number of effects. With the increase of n, CR of the PF configuration decreases while that of both the FF&PF and BF&PF configurations present irregular changes. What's more, CR of the PF configuration is always the lowest among the three feed configurations. On the premise of distillate production unchanged, the decrease of CR directly results in the increase of mass flow rate of feed seawater according to Eq. (19). Therefore, in the

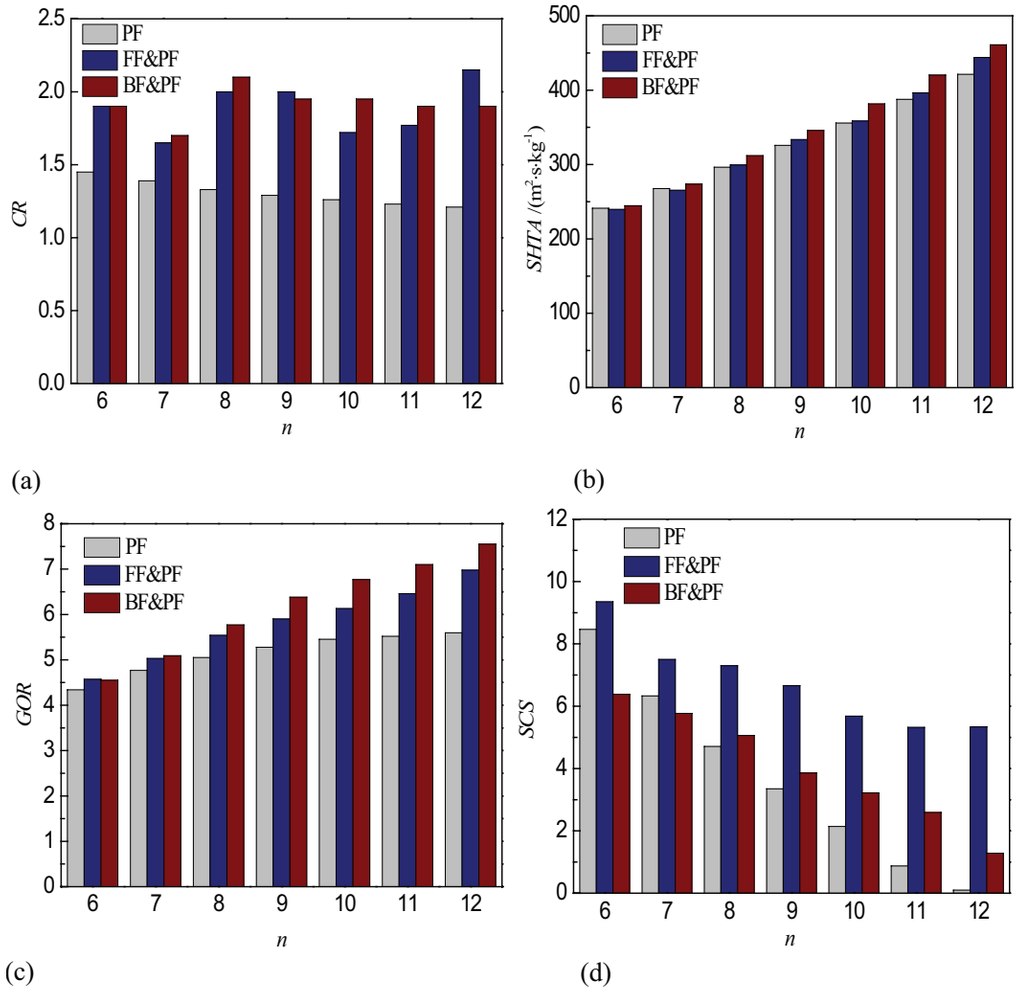

Fig. 7. Variations of CR with n and the feed configurations for T_{hs} = 70°C.

PF configuration, a reduced CR makes the mass flow rate of feed seawater into each effect enough to meet the limitations of spray density with the increase of n. As for both the FF&PF and BF&PF configurations, the mass flow rate of feed seawater into each effect is affected not only by the CR but also by the number of groups, which increases with the increase of n. Consequently, variations of the CR with n are irregular in the mixed feed configurations.

As shown in Fig. 7(b), SHTA of the three feed configurations increase with the increasing number of effects and wherein that of the BF PF configuration is the highest. The apparent temperature difference of each effect decreases with the increasing number of effects because the total apparent temperature difference of desalination plant remains the same. In the meanwhile, the effective temperature difference of each effect is reduced because the thermodynamic losses caused by the flow resistances and BPE ascend as the number of effects increases [17], which means that the driving force of heat transfer is weakened. Compared with the other feed configurations, the thermodynamic loss caused by BPE in the BF&PF configuration is exacerbated because of the high salinity occurring in evaporator/condenser with high evaporation temperature, and it results in the highest SHTA.

Fig. 7(c) displays that GOR of the three feed configurations increase as the number of effects increases. In addition, the BF&PF configuration and the PF configuration have the highest and the lowest GOR, respectively. The difference of GOR is more significant as the number of effects increases. Compared with the PF configuration, GOR of the FF&PF configuration increases by 4.8% and 24.7%, and that of the BF&PF configuration has the growth of 5.3% and 34.9% when n is 6 and 12.

The increasing number of effects raises the reusing rate of generated steam, which promotes the improvement of GOR. In the FF&PF configuration, the feed seawater is first supplied to the first effect of evaporator/condenser with the highest evaporation temperature, while it is fed to the last effect with the lowest evaporation temperature in the BF&PF configuration. Obviously, the subcooling degree of feed seawater (difference between the feed temperature and saturation temperature) in the FF&PF configuration is greater, which means more heat consumption used for preheating. Therefore, GOR of the FF&PF configuration is lower than that of the BF&PF configuration. Moreover, CR of the PF configuration is lower than the two mixed feed configurations according Fig. 7(a), and therefore, more consumption of heating steam is needed for preheating more amount of feed seawater.

As shown in Fig. 7(d), SCS of three feed configurations decreases with the increasing number of effects, and that of the FF&PF configuration is always the largest. Besides, SCS of the BF&PF configuration is the least when the number of effects is less than 8, but it is replaced by the PF configuration as the number of effects continues increasing.

On the premise of distillate production unchanged, the amounts of generated steam in each effect of the three feed configurations vary with the number of effects shown in Fig. 8. As the number of effects increases, the amount of generated steam in the last effect decreases, which reduces the cooling load of condenser. Therefore, the amount of seawater flowing into the condenser inlet decreases when the terminal difference of condenser remains the same. In addition, with the increase of sequence of effect, the amount of generated steam in each effect decreases first and then increases in the PF configuration, and that in the FF&PF configuration decreases in the first group and then increases in the subsequent groups while that in the BF&PF configuration decreases effect by effect. As a result, descending sort order of the amount of generated steam in the last effect of evaporator/condenser is FF&PF, PF and BF&PF, which means the reduction of cooling load of condenser. In the meantime, CR of the three feed configurations are different because of the limitation of spray density, which leads to the different amount of feed seawater. Therefore, under the combined effects of cooling load of condenser and amount of feed seawater, SCS of the three feed configurations exhibit such differences.

Fig. 9 presents the effects of temperature T_{hs} of heating steam on the performances of three feed configurations. The corresponding selected plans of FF&PF and BF&PF configurations are (4 + 2 + 2) and (2 + 3 + 3) for the 8-effect LT-MEE desalination plant. As shown in Fig. 9(a), CR of the three feed configurations increase with the rise of T_{hs}, and the increasing rate of CR of the two mixed feed configurations are significantly higher than the PF feed configuration. Moreover, CR of the BF&PF configuration is the highest and that of the PF configuration is the lowest. When both the length of heat transfer tube and row-column ratio of tube bundle remain the same, the number of columns decreases because SHTA reduces with the increase of T_{hs} as shown in Fig. 9(b). As a result, CR exhibits an increase trend to cut down the amount of feed seawater for insuring the proper spray density.

Variations of SHTA with the temperature T_{hs} of heating steam are shown in Fig. 9(b). It can be observed that SHTA of the three feed configurations decrease by deceleration. When T_{hs} rises from 56°C to 60°C, SHTA decreases by 24%. However, the decrement of SHTA is about 12% corresponding to the variation range of 68°C–72°C. In addition, SHTA of the BF&PF configuration is the largest in three feed configurations. Compared with it, SHTA of the FF&PF configuration has a decrease of 5% and that of the PF configuration decreases by 7%. On the premise that the number of effects and evaporation temperature in the last effect of evaporator/condenser remain constant, the average apparent temperature difference of heat transfer in each effect of evaporator/condenser increases with the rise of T_{hs} and then brings about the decrease of SHTA. With the increase of temperature difference, the overall heat transfer coefficient of HTE decreases [18], and BPE gets raised, so that the decrease rate of SHTA reduces gradually. The relationship of SHTA among the three feed configurations is corresponding to the CR because BPE is influenced by the CR and then has an effect on the effective temperature difference of heat transfer.

As demonstrated in Fig. 9(c), GOR of the three feed configurations decrease with the temperature T_{hs} of heating steam going up, and the BF&PF configuration obtains the highest GOR. When T_{hs} is 68°C, GOR of the FF&PF configuration is 9.3% higher than that of the PF configuration while that of the BF&PF configuration has an improvement of 15.2%. According to the physical properties of saturated steam, the latent heat of evaporation decreases with the

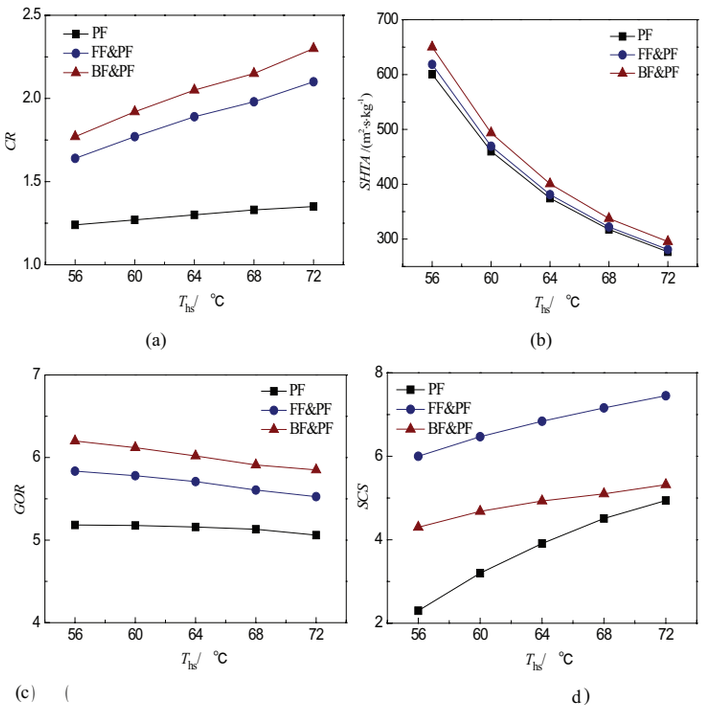

Fig. 8. Variations of $M_{d,i}$ with n and the feed configurations for T_{hs} = 70°C.

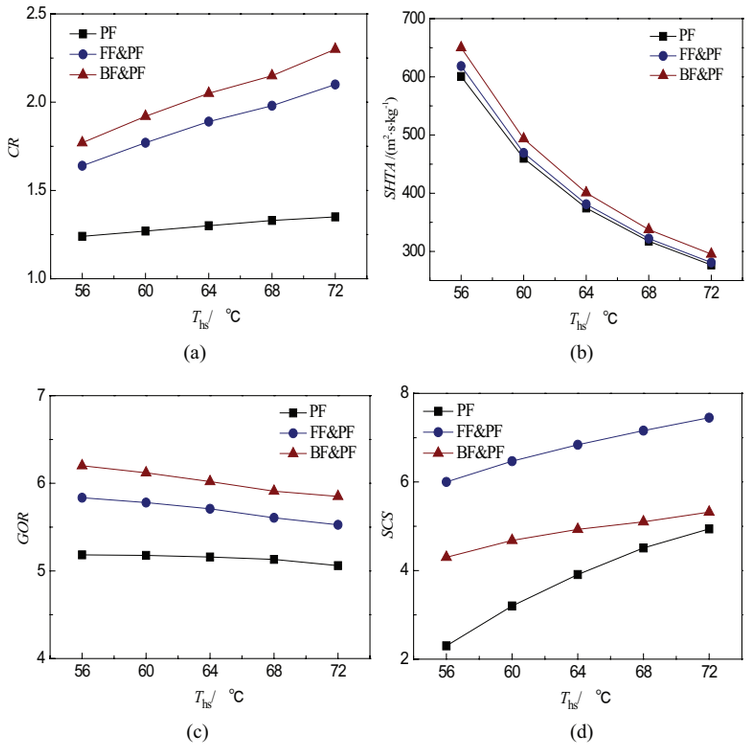

Fig. 9. Variations of CR with T_{hs} and the feed configurations for n = 8.

rise of saturated temperature. Furthermore, the subcooling degree of feed seawater increases with the increase of T_{hs}. Therefore, both of the two aspects make the required amount of heating steam increase, which results in the decrease of GOR.

Fig. 9(d) reveals the effect of the temperature T_{hs} of heating steam on SCS. SCS of the three feed configurations increase with the rise of T_{hs}. At the same temperature of heating steam, SCS of the FF&PF configuration is the largest, and the smallest one belongs to the PF configuration. With the growth of T_{hs}, the subcooling degree of feed seawater increases, and the increment is larger with the decrease of sequence of evaporator/condenser. Consequently, the generated steam in the last effect of evaporator/condenser increases with the increasing temperature of heating steam as demonstrated in Fig. 10, which means a lager cooling load of condenser. Besides, CR increases with the rise of T_{hs}. The two factors leads to the variation of SCS with the temperature of heating steam.

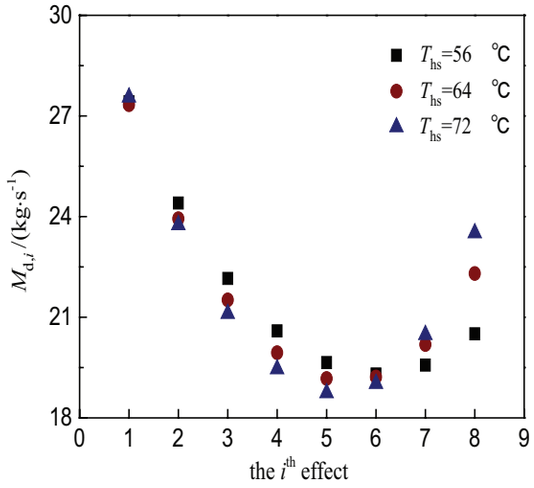

Fig. 10. Variation of $M_{d,i}$ with T_{hs} for n = 8 and PF configuration.

Fig. 11 shows the distributions of salinity and temperature of brine in the three feed configurations for n = 8 and T_{hs} = 72°C. It can be seen that with the rising sequence of evaporator/condenser, which means the fall of temperature, the salinity of brine in each effect of evaporator/condenser decreases first and then increases for the PF configuration, and that for the FF&PF configuration reduces in the first group and then gets raised in the subsequent groups while that for the BF&PF configuration decreases. This is caused by the differences of amount of generated steam in each effect of evaporator/condenser among the three feed configurations. In the process of evaporation, the salinity of brine forms the scale ($CaSO_4 \times 2H_2O$, $CaSO_4 \times 0.5H_2O$ and $CaSO_4$) on the surface of heat transfer tube due to thermal decomposition or form transformation. As for the three feed configurations in the calculation range of this paper, the maximum salinity of brine in ascending sort order is

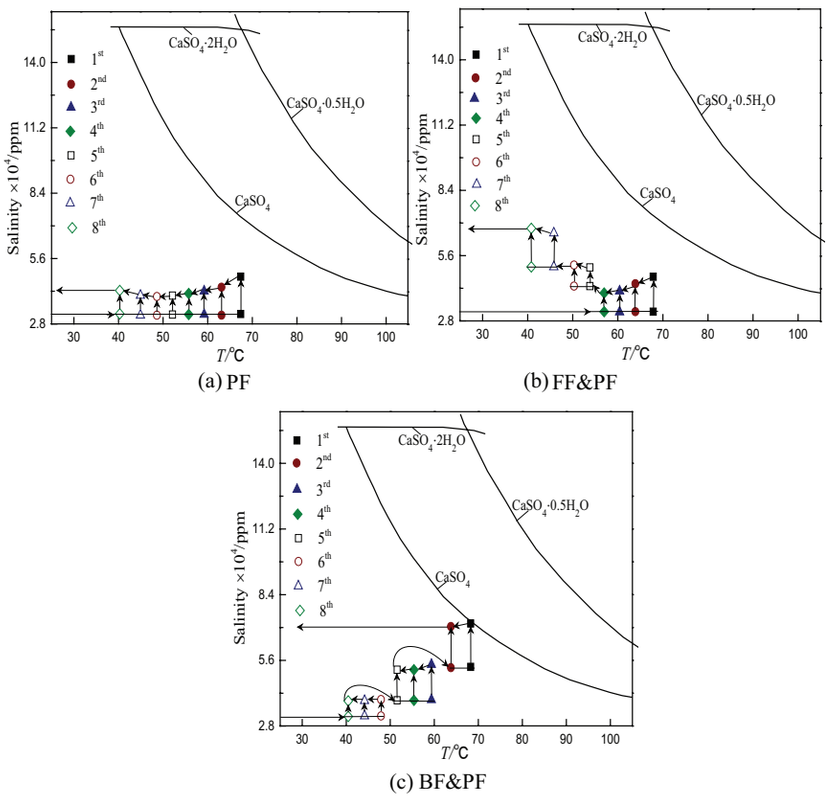

Fig. 11. Distributions of salinity and temperature for n = 8 and T_{hs} = 72°C.

PF (68.3°C, 48,000 ppm), FF&PF (40.4°C, 68,000 ppm) and BF&PF (68.3°C, 71,500 ppm), and that of the BF&PF configuration is very close to the solubility of $CaSO_4$ (68.3°C, 72,500 ppm), which indicates that scale risk of the BF&PF configuration is much higher than the other configurations.

5. Conclusions

On the basis of limiting the spray density, the effects of heating steam temperature and number of effects on the performance parameters were investigated, and the comparison of performance and scaling tendencies of various feed configurations were accomplished. Finally, the following points can be remarked within the calculation scope of this paper:

- As the number of effects increases, CR of the PF configuration decreases while that of both the FF&PF and BF&PF configurations present irregular changes. In addition, both SHTA and GOR increase, and SCS decreases for the three feed configurations.
- With the rising temperature of heating steam, CR increase and the increasing rates of the two mixed feed configurations are significantly higher than the PF feed configuration, and both SHTA and GOR decrease while SCS increases for the three feed configurations.
- Of the three feed configurations, the lowest GOR and CR belong to the PF configuration. Both SHTA and GOR of the BF&PF configuration are the highest. The difference of GOR is more significant as the number of effects increases. SCS of the FF&PF configuration is always the largest, and that of the BF&PF configuration is the least when the number of effects is less than 8, but it is replaced by the PF configuration as the number of effects continues increasing.
- With the rising sequence of evaporator/condenser, the salinity of brine in each effect decreases first and then increases for the PF configuration, and that for the FF&PF configuration reduces in the first group and then gets raised in the subsequent groups while that for the BF&PF configuration decreases. In the calculation range of this paper, the maximum salinity of brine in ascending sort order is PF, FF&PF and BF&PF, which indicates that scale risk of the BF&PF configuration is much higher than the other configurations.

Acknowledgments

Authors are grateful for the support of the Key Project of the National Natural Science Foundation of China (No. 51336001) and the National Key Technology R&D Program (2014BAB09B00).

Symbols

A	—	Area of heat transfer, m^2
BPE	—	Boiling point elevation, °C
c_p	—	Specific heat at constant pressure, kJ/kg•°C
CR	—	Concentration ratio
d	—	Diameter, m
g	—	Acceleration of gravity, m/s^2
GOR	—	Gained output ratio
h	—	Specific enthalpy, kJ/kg
K_{in}	—	Coefficient of heat transfer in condensation, W/m•°C
K_{out}	—	Coefficient of heat transfer in evaporation, W/m•°C
k	—	Coefficients of thermal conductivity, W/m•°C
L_t	—	Length of tube, m
M	—	Mass flow rate, kg/s
n	—	Number of evaporator/condenser
N	—	Number of tube column
R_{fou}	—	Resistance of fouling, m^2•K/W
SCS	—	Specific cooling seawater
SHTA	—	Specific heat transfer area, m^2•s/kg
T	—	Temperature, °C
U	—	Overall coefficient of heat transfer, W/m•°C
δT_{bun}	—	Temperature depression across the tube bundle, °C
δT_{con}	—	Temperature depression in the condensation process, °C
δT_{dem}	—	Temperature depression across the demister, °C
δT_{fri}, δT_{loc}	—	Temperature depression in vapor transmission channels, °C
X	—	Salinity, ppm

Greek letters

Γ	—	Spray density, kg/m s
η	—	Kinematic viscosity, m^2/s
λ	—	Latent heat, kJ/kg
μ	—	Dynamic viscosity, Pa/s
ξ	—	Resistance of thermal conductivity, m^2 °C/W
ρ	—	Density, kg/m^3

Subscripts

a	—	Average
b	—	Brine
b'	—	Accumulated brine
bf	—	Flashing of brine
bottom	—	Bottom row of tube bundle
c	—	Condensation
d	—	Distillate
df	—	Flashing of distillate
e	—	Evaporating phase
f	—	Feed
hs	—	Heating steam
l	—	Liquid
pre	—	Preheating phase
rej	—	Rejected
sw	—	Seawater
top	—	Top row of tube bundle
wall	—	Wall of tube

References

[1] G. Ruan, Thermal desalination in China, IDA J. Desal. Water Reuse, 5 (2013) 99–105.
[2] T. Mezher, H. Fath, Z. Abbas, A. Khaled, Techno-economic assessment and environmental impacts of desalination technologies, Desalination, 266 (2011) 263–273.
[3] N. Ghaffour, T.M. Missimer, G.L. Amy, Technical review and evaluation of the economics of water desalination: current and future challenges for better water supply sustainability, Desalination, 309 (2013) 197–207.
[4] H.T. El-Dessouky, H.M. Ettouney, F. Mandani, Performance of parallel feed multiple effect evaporation system for seawater desalination, Appl. Therm. Eng., 20 (2000) 1679–1706.
[5] M.A. Darwish, H.K. Abdulrahim, Feed water arrangements in a multi-effect desalting system, Desalination, 228 (2008) 30–54.
[6] M.A. Sharaf, A.S. Nafey, L. García-Rodríguez, Exergy and thermo-economic analyses of a combined solar organic cycle with multi effect distillation (MED) desalination process, Desalination, 272 (2011) 135–147.
[7] I.S. Al-Mutaz, I. Wazeer, Comparative performance evaluation of conventional multi-effect evaporation desalination processes, Appl. Therm. Eng., 73 (2014) 1194–1203.
[8] I.S. Al-Mutaz, Features of multi-effect evaporation desalination plants, Desal. Wat. Treat., 54 (2014) 3227–3235.
[9] A.D. Khawaji, I.K. Kutubkhanah, J.M. Wie, Advances in seawater desalination technologies, Desalination, 221 (2008) 47–69.
[10] S. Shen, X. Chen, X. Mu, Y. Wang, L. Gong, Heat transfer characteristics of horizontal tube falling film evaporation for desalination, Desal. Wat. Treat., 55 (2015) 3343–3349.
[11] S. Shen, S. Zhou, Y. Yang, L. Yang, X. Liu, Study of steam parameters on the performance of a TVC-MED desalination plant, Desal. Wat. Treat., 33 (2011) 300–308.
[12] S. Zhou, Y. Guo, X. Mu, S. Shen, Effect of design parameters on thermodynamic losses of the heat transfer process in LT-MEE desalination plant, Desalination, 375 (2015) 40–47.
[13] H.T. El-Dessouky, I. Alatiqi, S. Bingulac, H.M. Ettouney, Steady-state analysis of the multiple effect evaporation desalination process, Chem. Eng. Technol., 21 (1998) 437–451.
[14] S. Shen, R. Liu, Y. Yang, X. Liu, J. Chen, Condensation character of a stratified flow inside a horizontal tube, Desal. Wat. Treat., 33 (2011) 218–223.
[15] X. Mu, S. Shen, Experimental study of falling film evaporation heat transfer coefficient on horizontal tube, Desal. Wat. Treat., 50 (2012) 310–316.
[16] R. Deng, L. Xie, H. Lin, J. Liu, W. Han, Integration of thermal energy and seawater desalination, Energy, 35 (2010) 4368–4374.
[17] S. Shen, S. Zhou, X. Mu, Y. Guo, Analysis of thermodynamic losses of heat transfer process in large-scale LT-MED desalination plant, CIESC J., 65 (2014) 3366–3374.
[18] S. Shen, G. Liang, Y. Guo, R. Liu, X. Mu, Heat transfer performance and bundle-depth effect in horizontal-tube falling film evaporators, Desal. Wat. Treat., 51 (2013) 830–836.